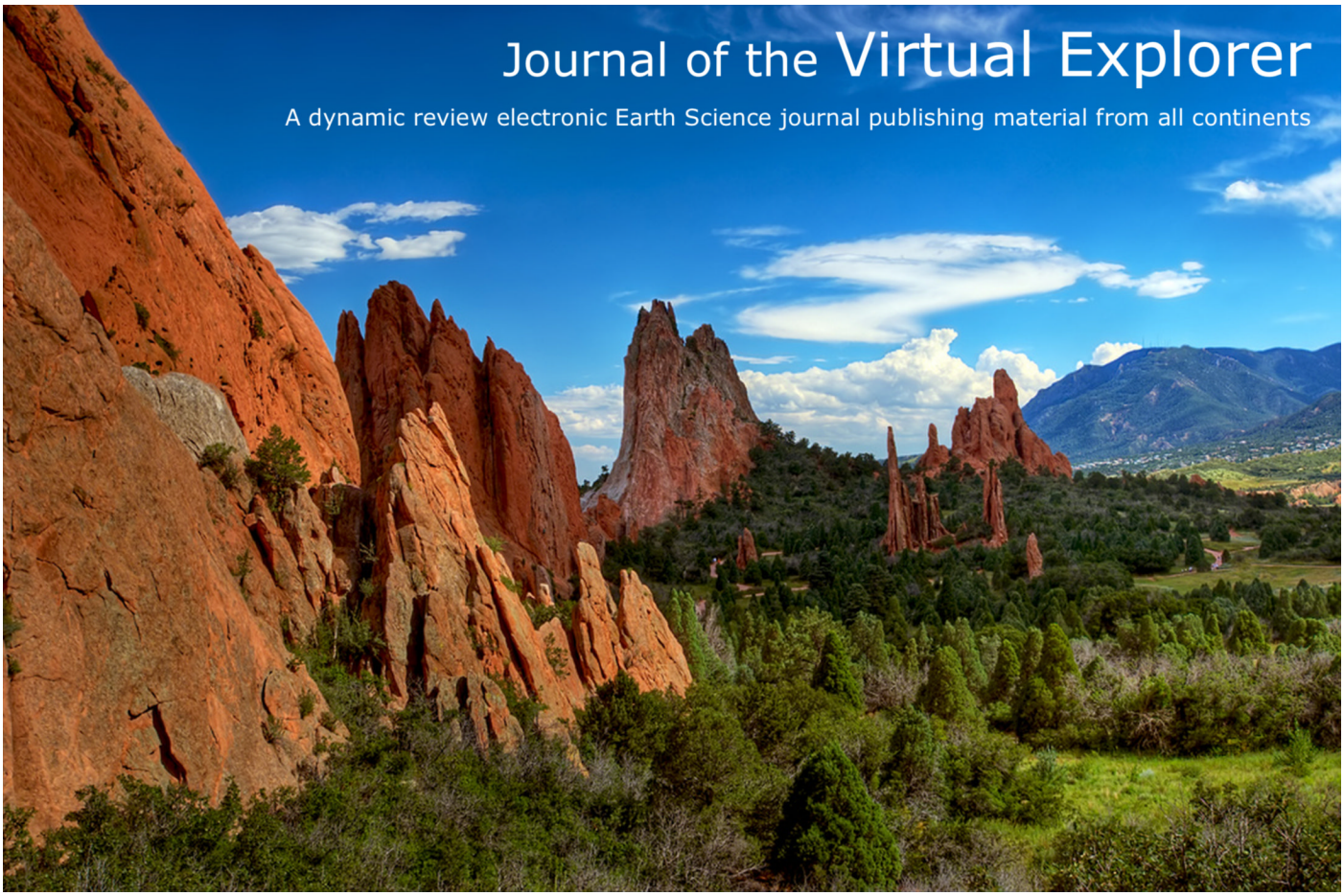

Geochemical characterizations of mafic magmatic rocks of the Central Indian Shield: Implication for Precambrian crustal evolution

Meraj Alam, Md. Naushad, Nishchal Wanjari, Talat Ahmad

Journal of the Virtual Explorer, Electronic Edition, ISSN 1441-8142, volume **32**, paper 8
In: (Eds.) Talat Ahmad, Francis Hirsch, and Punya Charusiri,
Geological Anatomy of India and the Middle East, 2009.

Geochemical characterizations of mafic magmatic rocks of the Central Indian Shield: Implication for Precambrian crustal evolution

Meraj Alam, Md. Naushad, Nishchal Wanjari, Talat Ahmad

Journal of the Virtual Explorer, Electronic Edition, ISSN 1441-8142, volume **32**, paper 8
In: (Eds.) Talat Ahmad, Francis Hirsch, and Punya Charusiri,
Geological Anatomy of India and the Middle East, 2009.

Abstract: Geochemical and petrogenetic studies have been conducted on a set of basaltic rocks from Betul, amphibolites and dolerite dykes which intrude the Tirodi and Amgaon Gneissic Complex from Betul-Chindwara and Amgaon regions respectively. Based on geochemical data the mafic volcanics are classified as basalt to basaltic andesite with tholeiitic lineage in the form of Fe-enrichment trend. All the rocks are distinctly enriched in incompatible trace elements including light rare earth elements (LREE) and large ion lithophile elements (LILE), with continental signature in the form of negative Nb, P and Ti anomalies in their primitive mantle-normalised spidergrams. These chemical characteristics indicate their derivation from enriched mantle sources / sub-continental lithosphere.

The dykes traversing the Tirodi Gneissic Complex (TGC) in Chhindwara region have high abundances of Fe-oxides and alkali elements. Petrographic studies show that majority of the samples depict two generations of mineral growth. First generation has primary phases including olivine, pyroxene, plagioclase and the second generation has palagonite and leached Fe-oxides. These dykes are sub-alkaline, ranging in composition from basalt to basaltic andesite, with tholeiitic affinity. Doleritic dykes of TGC have enriched light rare earth elements (LREE) pattern and large ion lithophile elements (LILE) with depleted high field strength elements (HFSE) which probably indicate their derivation by partial melting of enriched mantle sources, while the dykes of Amgaon Gneissic Complex (AGC) have lower LREE-LILE abundances and with less enriched REE and multi-element patterns, which probably indicate higher degrees of partial melting of similarly enriched sources. Negative Sr-anomaly is conspicuous, probably indicating role of plagioclase fractionation in their genesis.

http://virtualexplorer.com.au/article/2009/246/geochemical-characterizations-of-mafic-magmatic-ro

Citation: Alam, M., Naushad, M., Wanjari, N., Ahmad, T. 2009. Geochemical characterizations of mafic magmatic rocks of the Central Indian Shield: Implication for Precambrian crustal evolution. In: (Eds.) Talat Ahmad, Francis Hirsch, and Punya Charusiri, *Journal of the Virtual Explorer*, volume **32**, paper 8, doi: 10.3809/jvirtex.2009.00246

Introduction

The Proterozoic era representing about half of the record earth history ranging in age from 2500 to ~550 Ma (Pharaoh *et al.*, 1987), is of great significance in understanding the evolution of Earth's crust. This period is characterized by the development of stable cratons which behaved as internally rigid crustal units similar to modern lithospheric plates (Windley, 1982). Recent data on composition of volcanic rocks, sedimentary facies, and structural trends and ore association suggest that different components of Proterozoic crust were formed in different tectonic settings, although the identification of such tectonic setting is still an enigma. The highly variable composition of early Proterozoic crust suggests a drastic change in the growth of the continental crust at the dusk of Archaean period (Naqvi, 1981; Taylor and McLennan, 1985; Pharaoh *et al.*, 1987).

The occurrence of Archaean type lithological units along with practically unique and new lithological elements in the early Proterozoic crust assemblages suggests that the Archaean-Proterozoic boundary represents a transitional period (Cloud, 1976; Taylor, 1987). This boundary is characterized by diachronous successive stabilization of cratons and considered as one of the major crust forming events in the earlier history of the earth (Moorbath, 1977; McCulloch and Wasserburg, 1978; Taylor, 1987). It is believed that towards the end of the Archaean, the major changes in global tectonic were related to cooling (Bickle, 1990, Ahmad and Rajamani, 1991) which is evident from the relatively less abundant occurrences of komatiites and related rocks in early Proterozoic terrains. The large volume of komatiites in Archaean terrains indicate presence of higher temperature and extents of partial melting prevailing during that period, giving rise to mantle plume related magmatism during the Archaean (White and McKenzie, 1989; Bickle, 1990; Campbell and Griffiths, 1990), and changing patterns of convection system (Hargraves, 1981; Bickle, 1990).

The possible role of plate tectonics during Proterozoic has received much attention by the geologists (Kroner, 1981; Schweitzer and Kroner, 1985; Condie, 1986 and 1989) and it is now widely accepted that the Precambrian plate tectonic process was similar to those operating today. The only differences may be in the size of plates (Tarney and Windley, 1977). Since certain characteristics of mafic magmatic rocks are considered to be related to their tectonic settings, geochemical studies of these rocks can give clues about petrogenetic processes and tectonic settings at the time of their emplacement. Therefore, the geochemical characteristics of mafic magmatic sequences coupled with geochronological and other field controls can provide better constraints to evaluate the evolution of mantle through time, possible mantle heterogeneities and petrogenetic processes (Condie, 1985 and 1989).

Geological setting of the study area

The Central Indian Tectonic Zone (CITZ) is an important, continental scale tectonic zone of Proterozoic age. It divides Indian continental shield into two tectono-magmatic provinces, the northern crustal province comprising Bundelkhand craton and the southern peninsular crustal province comprising Bastar, Dharwar and eastern Singhbhum craton (Stein *et al.*, 2004; Acharyya and Roy, 2000). CITZ is over 1600km. long with width up to 200km (Stein *et al.*, 2004), and is bounded by lineaments called Son-Narmada North Fault (SNNF) in the north and Central Indian Shear (CIS) in the south (Fig. 1a). In between these extreme boundaries two more lineaments have been identified as Son-Narmada South fault (SNSF) and Gavilgarh-Tan Shear Zone (GTSZ) (Yedekar, 1990; Jain, 1991). The rocks exposed in the study area comprise Amgaon Gneissic Complex (AGC), Tirodi Gneissic Complex (TGC) of ~2500-2200 Ma old and Betul supra crustal sequences. Whole rock Sm-Nd isochron age for the acidic volcanic rocks of Sakoli bimodal volcanic, south of the CIS, has given the age of crystallization at ca. 1675±180 Ma (Ahmad *et al.* 2009).

The Betul-Chindwara belt forms a conspicuous lithotectonic unit composed of volcano-sedimentary succession intruded by mafic-ultramafic and granitic suite of rocks. Amgaon and Tirodi Gneissic Complex have mafic magmatic rocks in the form of volcanic flows, amphibolites and doleritic dykes of distinct entities. Most of these dykes are probably of Paleo-Mesoproterozoic age, as they do not traverse through the overlying younger stratigraphic sequence. We have studied the mafic dykes and flows from distinct lithological packages, covering large area to understand their nature, evolutionary trends in terms of petrography, geochemical characteristics and their petrogenesis. These in turn will help us understand the nature of the Precambrian sub-continental mantle source that gave rise to the volcanics and dykes in the CITZ and its immediate south across the CIS (Fig.1).

Figure 1. Outline Geological Map of the Indian Shield (inset) and the Central Indian Shield

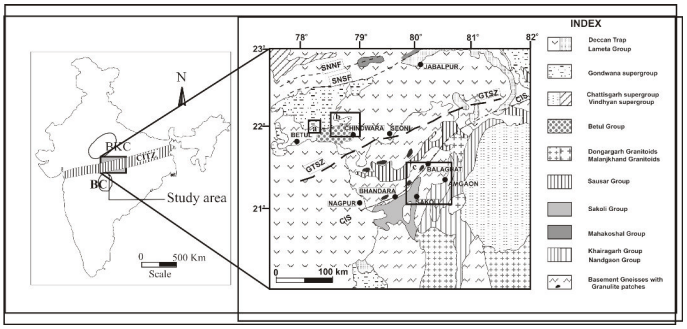

Map Showing the regional geology of the study area along with the disposition of major lineaments and Super-groups along the Central Indian Suture (modified after Roy and Ramachandra, 2003) Inset map of India showing outline of the Central Indian Tectonic Zone.

The Betul belt is overlain by Gondwana sediments and Deccan Trap on all three sides, but for a narrow corridor near Kanhan River through which it is connected to the CITZ basement. TGC, volcano-sedimentary sequence, younger metasediments, acid and basic intrusive of Archaean to Neo Proterozoic age occupies the north-eastern and northern part of the study area. Amla Gneiss of the TGC is the oldest litho-unit, exposed ~16km southwest of Betul town. The rocks range in age from Mesoproterozoic to Quaternary, the basaltic lava flows of Deccan traps are well exposed in the eastern and southern part. Numerous E-W trending dykes and sills mostly of mafic composition are exposed. They range in length from a few hundred meters to several kilometers, width ranging from a few meters to a few hundred meters. TGC includes the migmatites and basement gneiss/older migmatite (Fig. 1b). The migmatite comprise at least two phases of migmatization of which one involving partial migmatization of Sausar sediments has been dated to be about 1525±70 Ma (Sarkar *et al.* 1986). The AGC includes the migmatite/gneiss exposed south of the CIS, characterised by numerous amphibolites, dolerite, basic and ultrabasic intrusive. Like the TGC, the AGC also exhibits multiple mafic magmatic episodes (Fig. 1c).

Figure 1a. Geological map around Betul area

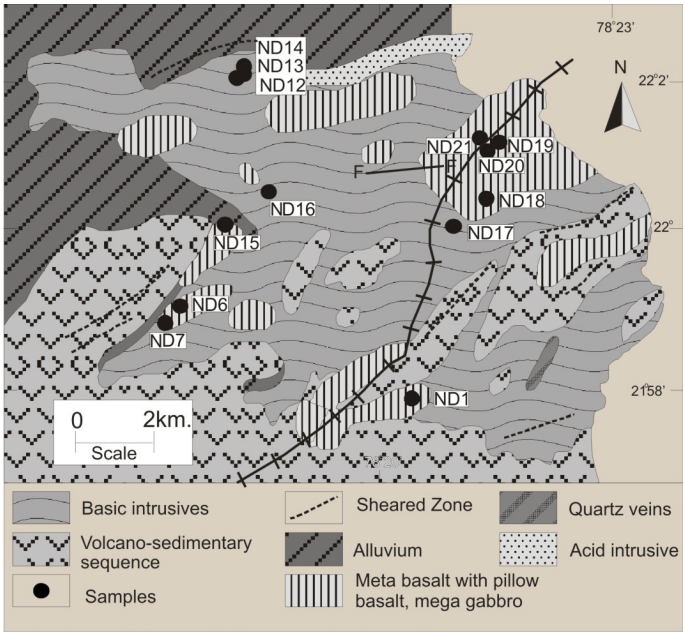

Geological map of Betul area with sample location. Map modified after district resource map (Geology and Minerals)-Betul district, M.P, Geological Survey of India (Central region).

Figure 1b. Geological map around Chindwara area

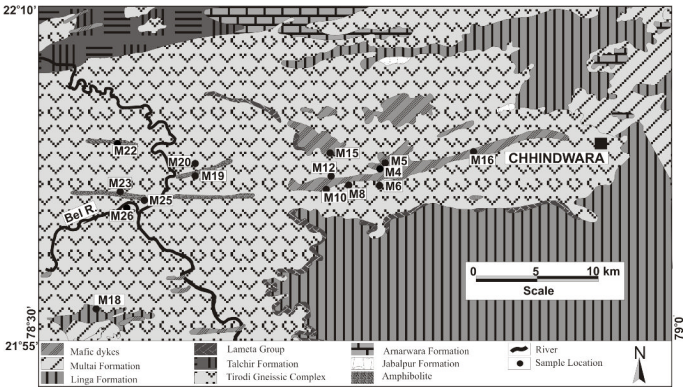

Geological map showing location of the mafic magmatic dyke from Tirodi Gneissic Complex (TGC) around Chhindwara region. (Modified after District Resource Map, GSI).

Figure 1c. Geological map around Amgaon area

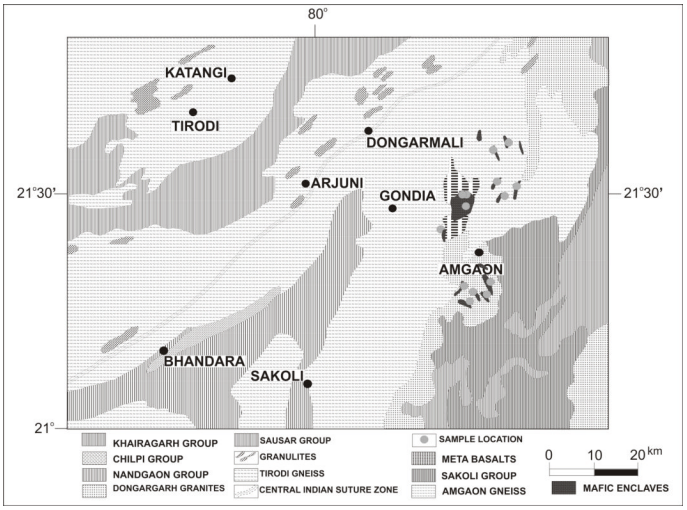

Geological map Amgaon area showing the mafic magmatic bodies and sample locations in the Amgaon Gneissic Complex (AGC) (modified after Yedekar *et al.*, 2003).

Petrographic character

The doleritic rocks show ophiotic to sub ophiotic texture. Characteristically leached iron stains are present along the opaque minerals. The sample of amphibolites shows a holocrystalline rock that has subhedral to euhedral plagioclase (sodic and calcic) grains and Fe-oxides are present as essential phase while quartz and pyroxenes are present as accessory minerals. Some samples show normal lamellar twins that may have developed due to the cubic-tetragonal transition of the mineral, while some samples show the intergrowth of the plagioclases crystals. The leaching of the Fe-oxide grains is very prominent that shows the 2nd phase of paragenesis. Some plagioclase grains show sericitization.

In the amphibolites samples hornblende, plagioclase, clinopyroxene and Fe-oxides are present as essential minerals; quartz and mica (biotite) grains are present as accessory minerals. Schistosity is well developed; thin sections show ophiotic to subophiotic texture. Albitization of pyroxene grains is very prominent in some sections. In a majority of the thin sections two phases of mineral formation are observed, one phase has palagonite formation and the other represents leaching of Fe-oxides. The plagioclases are two generations. One that is older shows more calcic phases and the later one more sodic nature which probably indicates the sodic metasomatism of the sample or enrichment of sodium from the outer sources.

The samples of Betul mafic volcanic rocks show an inequigranular, subhedral to euhedral, holo-crystalline to hypo-crystalline texture. These rocks have plagioclase (sodic and calcic), pyroxene and Fe-oxide as essential minerals while quartz and plagioclase in ground mass are present as accessory minerals. Ground mass is granular composed of plagioclase, quartz and volcanic glass. The palagonite (characteristically) is the alteration product of basaltic glass, which probably formed by hydration and devitrification process. Dissolution contacts around the palagonite grains are prominent in some samples.

Geochemistry

Analytical techniques

Basalt, amphibolite and dolerite dyke samples, collected from wide spread localities from the study area (Fig. 1a, 1b and 1c) were broken into small pieces using steel mortar. These were then reduced into small chips using jaw crusher. These were thoroughly washed, air dried and homogenised before making fine powder of -230 mesh using agate mills. The fine powdered samples were used for the analysis of major and trace elements including the rare earth elements at NGRI, Hyderabad. Major elements were determined by X-ray fluorescence spectrometry (XRF) (Philips Magix Pro Model 2440). Trace elements including the Rare Earth Elements (REE) were analysed using ICP-MS (Perkin Elmer, Sciex Elan DRC II). The procedure for major and trace analyses is described in Balaram *et al.* (1996). The analytical data are listed in Tables 1-3.

Table 1. Major element (wt%) and trace elements (in ppm) for Betul Mafic Volcanics

Samples	ND1	ND06	ND07	ND12	ND13	ND14	ND15	ND16	ND17	ND18	ND19	ND20	ND21
SiO_2	51.89	48.46	53.29	50.19	49.25	49.33	48.99	44.88	49.99	51.74	56.03	49.98	53.9
Al_2O_3	8.99	11.72	11.07	13.55	12.93	12.33	11.48	9.92	12.96	12.31	10.58	9.78	12.91
Fe_2O_3	11.98	13.06	11.96	12.49	14.02	14.59	12.89	16.49	11.9	13.12	10.95	12.76	12.47
MnO	0.25	0.2	0.18	0.16	0.16	0.18	0.17	0.22	0.17	0.18	0.2	0.18	0.17
MgO	9.68	9.99	7.4	7.06	7.65	7.21	9.74	18.94	8.07	7.71	5.59	9.46	6.81
CaO	12.58	12.23	10.26	10.45	10.09	11.33	13.48	7.66	12.53	9.8	10.97	14.33	8.08
Na_2O	1.33	1.46	2.9	1.99	1.73	1.83	1.1	0.19	1.75	2.77	2.6	0.65	3.16
K_2O	0.67	0.47	0.21	0.86	1.14	0.65	0.3	0.12	0.5	0.35	0.27	0.49	0.17
TiO_2	0.64	0.72	0.89	1.18	1.24	1.26	0.72	0.43	0.66	0.67	0.8	0.77	0.56
P_2O_5	0.19	0.2	0.18	0.25	0.22	0.18	0.1	0.08	0.11	0.13	0.14	0.12	0.03
LOI	2.31	1.51	1.68	1.02	0.89	0.97	0.78	0.82	1.62	0.87	2.02	1.73	1.6
Total	100.51	100.02	100.02	99.2	99.32	99.86	99.75	99.75	100.26	99.65	100.15	100.25	99.86
Trace Elements													
Sc	28	28	43	33	34	41	35	22	33	39	38	33	36
V	171	190	225	203	273	337	224	142	215	216	212	199	204
Cr	422	92	183	58	82	75	219	389	111	92	73	83	79
Co	68	38	52	42	46	43	61	75	40	46	47	33	49
Ni	574	101	98	68	72	57	193	582	73	65	49	44	64
Cu	22	46	66	102	127	103	143	16	83	81	45	22	20
Zn	108	64	72	58	60	68	63	53	50	64	68	53	51
Ga	12	14	12	18	17	18	13	9	14	15	12	16	11
Rb	7	10	3	10	9	8	4	2	5	5	5	11	2
Sr	259	280	98	260	203	212	217	23	237	240	272	112	230
Y	17	20	20	24	22	21	14	12	15	17	21	19	16
Zr	65	61	75	114	90	91	41	23	49	57	83	53	58
Nb	3	2	4	5	3	5	2	5	4	4	4	4	3
Ba	351	110	124	388	319	357	295	92	121	190	114	99	144
La	26.01	6.63	11.33	13.66	9.93	9.49	4.77	6.95	7.36	7.31	9.72	7.81	4.88
Ce	50.09	13.66	24.88	28.94	21.01	20.85	10.53	14.15	15.35	15.29	21.40	15.37	10.48
Pr	4.61	1.53	2.65	3.01	2.22	2.24	1.12	1.48	1.58	1.62	2.28	1.64	1.23
Nd	22.52	9.11	14.89	16.65	12.63	12.45	6.30	7.39	8.48	9.09	12.76	8.93	7.51

Samples	ND1	ND06	ND07	ND12	ND13	ND14	ND15	ND16	ND17	ND18	ND19	ND20	ND21
Sm	3.70	2.15	3.05	3.38	2.75	2.92	1.57	1.41	1.75	1.96	2.85	1.97	1.80
Eu	1.12	0.90	0.86	1.41	1.17	1.21	0.72	0.60	0.76	0.77	0.87	0.70	0.75
Gd	4.97	2.86	3.97	4.75	3.80	4.01	2.20	1.97	2.45	2.87	4.00	2.88	2.45
Tb	0.54	0.45	0.57	0.67	0.57	0.60	0.36	0.26	0.38	0.45	0.58	0.43	0.40
Dy	2.38	2.49	3.04	3.53	2.97	3.18	2.09	1.34	2.12	2.45	3.20	2.47	2.19
Ho	0.47	0.54	0.63	0.71	0.62	0.68	0.46	0.31	0.47	0.54	0.69	0.55	0.47
Er	1.70	1.88	2.16	2.37	2.00	2.16	1.56	1.04	1.52	1.78	2.28	1.83	1.47
Tm	0.27	0.31	0.35	0.39	0.31	0.36	0.27	0.18	0.25	0.29	0.37	0.29	0.25
Yb	1.39	1.63	1.81	2.05	1.73	1.97	1.42	1.01	1.41	1.68	2.13	1.67	1.37
Lu	0.21	0.25	0.27	0.30	0.26	0.28	0.22	0.16	0.22	0.24	0.32	0.26	0.20
Pb	2.44	3.70	3.77	2.81	2.52	3.27	9.31	2.38	2.87	4.17	3.93	7.39	2.48
Th	3.49	0.46	1.50	1.63	0.97	1.14	0.62	0.73	0.82	1.05	1.44	0.95	0.79
U	1.21	0.57	0.82	0.58	0.53	0.65	0.77	0.54	0.53	0.74	0.69	0.94	0.38
Mg#	47.31	45.95	40.75	38.58	37.75	35.45	45.65	56.07	42.98	39.51	36.20	45.17	37.77

Table 2. Major element (wt%) and trace elements (in ppm) for amphibolite and dolerite dykes from TGC

Samples	M4	M5	M6	M8	M10	M12	M13	M16	M18	M19	M20	M22	M23	M25	M26
SiO_2	50.42	49.58	48.2	52.93	49.81	49.95	49.91	51.97	48.67	56.19	50.7	54.1	53.97	48.05	55.45
Al_2O_3	13.7	13.39	13.61	10.92	12.67	13.7	13.2	12.54	12.23	13.67	12.54	13.19	12.33	13.84	12.53
Fe_2O_3	13.98	14.7	13.71	13.2	15.32	13.65	14.38	14.73	16.22	8.58	11.99	10.78	12.41	10.65	9.46
MnO	0.17	0.18	0.17	0.16	0.21	0.16	0.17	0.17	0.18	0.11	0.16	0.13	0.15	0.15	0.15
MgO	5.18	5.26	5.1	5.48	5.27	5.8	5.03	4.48	5.81	5.12	7.71	5.57	5.6	10.34	5.79
CaO	9.99	10.09	10.13	11.56	9.18	10.26	9.94	8.57	9.95	4.61	13.44	5.61	9.95	13.46	13.28
Na_2O	2.41	2.34	2.4	1.75	2.34	2.16	2.22	2.27	1.99	2.37	0.74	2.13	2.74	0.94	0.79
K_2O	0.67	0.7	0.64	0.42	1.04	0.78	0.72	0.87	0.4	4.78	0.29	3.75	0.31	0.18	0.24
TiO_2	2.13	2.26	2.14	2.02	2.73	1.96	2.17	2.54	2.36	2.22	0.7	2.19	0.66	0.46	0.62
P_2O_5	0.25	0.26	0.24	0.16	0.37	0.26	0.29	0.36	0.29	1.07	0.12	0.82	0.11	0.11	0.24
LOI	1.49	1.59	1.5	1.67	1.84	1.15	1.89	1.86	2.87	0.49	0.68	0.92	0.81	1.07	0.51
Total	100.39	100.35	97.84	100.27	100.78	99.83	99.92	100.36	100.97	99.21	99.07	99.19	99.04	99.25	99.06
Trace Elements															
Sc	33	30	34	25	30	32	32	30	34	15	18	16	40	27	34

Samples	M4	M5	M6	M8	M10	M12	M13	M16	M18	M19	M20	M22	M23	M25	M26
V	350	315	356	266	293	339	335	368	390	151	184	156	223	130	221
Cr	51	37	42	35	35	38	41	35	42	31	25	31	113	178	119
Co	47	42	49	36	44	46	45	43	51	23	27	23	52	47	39
Ni	31	26	29	23	24	27	27	22	28	15	15	16	35	50	34
Cu	214	194	213	214	278	210	195	265	229	59	51	50	34	32	49
Zn	116	115	100	75	104	97	94	109	101	89	87	89	101	44	53
Ga	25	22	25	16	24	23	23	25	25	23	23	22	19	12	18
Rb	14	14	11	7	21	15	12	20	6	105	86	109	5.0	2	5
Sr	245	232	248	193	225	237	232	177	201	608	599	367	189	136	153
Y	21	22	20	19	28	21	21	28	19	55	52	62	14	8	11
Zr	112	112	109	118	166	116	124	152	93	379	344	299	49	18	32
Nb	25	20	22	18	30	19	22	20	15	51	56	45	6	2	3
Ba	247	312	236	255	280	248	208	198	161	160	157	95	195	94	117
La	17.72	17.42	17.67	13.71	22.52	16.08	17.35	19.65	13.95	129.26	99.65	73.18	9.37	3.49	7.54
Ce	41.00	39.06	39.92	31.35	51.19	36.97	38.45	44.90	32.27	239.56	194.50	140.83	19.89	7.37	15.67
Pr	4.39	4.12	4.28	3.43	5.47	4.04	4.19	4.88	3.64	21.39	17.66	13.02	2.19	0.78	1.60
Nd	24.65	23.27	24.36	19.48	31.23	22.97	23.61	28.20	21.50	96.16	82.23	61.90	11.88	4.18	8.56
Sm	5.55	5.08	5.33	4.31	6.68	5.16	5.12	6.67	5.31	12.99	11.86	9.74	2.68	1.00	2.00
Eu	1.91	1.75	1.91	1.53	2.27	1.85	1.80	2.16	1.89	3.53	3.40	2.53	0.97	0.44	0.74
Gd	7.29	6.95	7.14	5.70	9.05	7.02	6.97	8.90	7.06	19.42	16.97	14.11	3.92	1.42	2.82
Tb	1.05	0.98	1.06	0.81	1.29	0.99	1.02	1.35	1.08	1.70	1.63	1.50	0.61	0.22	0.43
Dy	5.25	4.86	5.26	4.17	6.35	4.90	5.03	6.88	5.57	6.29	6.23	6.34	3.35	1.22	2.30
Ho	1.06	0.96	1.09	0.81	1.28	1.00	1.02	1.44	1.13	1.18	1.22	1.28	0.73	0.27	0.54
Er	3.38	3.00	3.38	2.59	4.02	3.15	3.027	4.37	3.57	4.04	4.13	4.18	2.49	0.90	1.79
Tm	0.53	0.48	0.53	0.41	0.62	0.50	0.50	0.72	0.56	0.52	0.56	0.63	0.43	0.16	0.32
Yb	2.95	2.62	2.93	2.21	3.35	2.67	2.79	3.88	3.11	2.89	3.11	3.46	2.36	0.82	1.78
Lu	0.44	0.38	0.43	0.32	0.50	0.39	0.42	0.56	0.46	0.41	0.45	0.52	0.36	0.13	0.28
Pb	4	4	3	6	2	3	4	3	2	7.5	5.5	5.0	4.6	2.5	2.6
Th	2	2	2	2	3	2	2	2	2	8.4	4.4	6.9	1.4	0.5	1.2
U	2	2	2	3	2	1	2	2	2	2.5	2.0	2.0	1.7	0.6	1.6
Mg#	44.26	28.45	45.09	31.57	27.65	32.07	27.99	39.27	28.47	39.87	41.68	36.47	47.12	51.9	40.48

Table 3. Major element (wt%) and trace elements (in ppm) for amphibolite and dolerite dykes from AGC

Samples	S1	S2	S6	S10	S11	S15	S19	S20	S21	S22	S23	S25	S33	S34
SiO_2	49.63	49.18	50.83	49.89	47.47	48.55	47.24	47.95	46.01	49.79	49.66	47.41	48.37	48.65
Al_2O_3	13.67	13.53	8.08	13.23	11.83	11.33	11.23	11.83	10.07	11.54	12.2	10.47	11.53	11.8
Fe_2O_3	14.28	14.33	11.79	15.27	15.77	17.55	16.56	15.29	16.47	14.07	14.77	15.7	16.96	17.51
MnO	2.41	2.37	1.24	2.24	1.81	2.2	2.86	2.53	2.46	3.3	3.79	2.71	1.95	2.34
MgO	6.01	5.93	11.36	5.85	5.75	6.3	5.28	6.16	6.8	6.27	5.81	5.12	6.73	6.03
CaO	0.29	0.3	0.52	0.57	0.46	0.4	0.2	0.19	0.09	0.14	0.14	0.21	0.33	0.72
Na_2O	10.54	10.47	11.9	10.24	9.99	10.04	10.46	9.71	9.58	11.58	8.42	10.05	9.96	9.12
K_2O	0.2	0.2	0.14	0.22	0.21	0.23	0.23	0.19	0.19	0.27	0.19	0.23	0.22	0.24
TiO_2	1.74	1.7	0.94	1.47	1.21	1.08	1.66	1.42	1.69	1.59	2.04	1.4	0.92	1.22
P_2O_5	0.21	0.22	0.01	0.1	0.1	0.17	0.14	0.13	0.14	0.12	0.16	0.11	0.14	0.17
LOI	0.79	0.69	1.45	0.76	1.04	1.07	1.59	0.4	1.29	0.54	0.65	0.34	0.82	0.96
Total	99.77	98.92	98.26	99.84	95.64	98.92	97.45	95.8	94.79	99.21	97.83	93.75	97.93	98.76
Trace Elements														
Sc	44	45	52	44	44	46	38.2	45.9	39.7	44.5	48.6	43	43	42
V	327	334	343	290	290	284	350	375	361	378	370	358	359	318
Cr	234	269	538	276	276	123	124	209	197	199	276	198	191	214
Co	52	51	31	53	53	20	43	24	19	22	48	39	45	43
Ni	161	210	172	214	214	39	115	35	31	42	101	72	130	131
Cu	97	93	45	190	190	23	186	20	25	75	66	92	229	182
Zn	100	101	76	113	113	59	128	85	64	75	142	118	125	119
Ga	21	18	11	19	19	10	18	13	11.1	10	16	18	18	16
Rb	10	9	6	22	22	8	31.6	4.6	3.8	1.4	4.3	3.4	9	9
Sr	216	193	143	143	143	68	102.6	81.7	88.4	65.5	121.3	109.6	106	99
Y	45	41	10	42	42	20	53.3	28.8	20.3	26.4	42.0	41.6	43	41
Zr	114	110	36	90	90	46	108.3	66.1	52.2	68.2	102.8	111.8	96	93
Nb	7	8	3	7	7	3	5.0	4.4	3.6	4.2	6.3	7.2	6	5
Ba	264	201	111	164	164	120	199	36	30	22	94	91	144	98
La	12.06	11.7	12.26	9.17	9.2	8.35	6.66	6.22	4.20	6.54	6.27	2.9	5.70	6.64
Ce	28.34	28.13	28.59	21.33	21.33	18.33	19.48	18.44	14.3	20.12	17.8	9.93	16.3	16.13
Pr	3.96	3.9	4.56	2.87	2.87	2.49	2.68	2.95	2.26	3.22	2.81	1.963	2.44	2.48

Samples	S1	S2	S6	S10	S11	S15	S19	S20	S21	S22	S23	S25	S33	S34
Nd	16.95	16.26	20.5	12.11	12.11	10.22	11.87	14.24	11.1	15.52	13.63	9.94	11.1	10.7
Sm	4.63	4.5	5.16	3.32	3.32	2.93	3.71	4.33	3.45	4.45	4.05	3.48	3.54	3.22
Eu	1.62	1.54	1.45	1.17	1.17	1.1	1.25	1.5	1.13	1.38	1.35	1.18	1.22	1.11
Gd	5.43	5.32	4.76	4.06	4.06	3.77	4.5	5.13	4.1	5.35	4.73	4.26	4.37	4.13
Tb	0.91	0.9	0.62	0.72	0.72	0.71	0.79	0.92	0.73	0.94	0.82	0.78	0.79	0.74
Dy	5.51	5.45	2.84	4.5	4.5	4.55	5.01	5.64	4.61	5.82	5.2	4.8	5.12	4.74
Ho	1.16	1.15	0.49	0.99	0.99	1.02	1.08	1.25	1.01	1.28	1.16	1.08	1.14	1.04
Er	3.09	3.00	1.14	2.61	2.61	2.78	2.9	3.32	2.63	3.44	3.06	2.814	3.11	2.87
Tm	0.47	0.47	0.15	0.42	0.42	0.45	0.45	0.5	0.39	0.52	0.45	0.43	0.5	0.47
Yb	3.02	3.01	0.87	2.77	2.77	2.94	2.95	3.31	2.62	3.46	2.96	2.82	3.32	3.07
Lu	0.45	0.45	0.12	0.42	0.42	0.44	0.44	0.496	0.39	0.51	0.435	0.42	0.5	0.47
Pb	3.5	2.0	5.8	5.3	5.3	4.0	1.9	8.3	3.8	2.9	12.3	6.3	7.6	5.5
Th	2.0	2.1	2.1	2.3	2.3	2.5	1.0	4.0	0.5	0.5	0.5	0.5	1.1	1.2
U	1.0	1.0	0.5	0.6	0.6	0.5	0.4	0.1	0.1	0.1	0.1	0.1	0.2	0.2
Mg#	31.84	31.52	51.71	29.86	28.84	28.51	26.17	30.91	31.46	33.1	30.41	26.59	30.61	27.66

Alteration and elemental mobility

It is widely recognized that in Precambrian rocks some of the elements are mobile during alteration and metamorphism. For this reason, we have tried to select the least altered samples for geochemical analyses. Ternary CaO/Al_2O_3-$MgO/10$-$SiO_2/100$ diagram (after Schweitzer and Kroner, 1985); which is widely used to distinguish between altered and unaltered rocks, a majority of the samples plot in the field of unaltered basalts (Fig. 2). Although the REE are considered to be somewhat mobile during alteration (Ludden and Thompson, 1979), the regularity of REE patterns in all the studied samples suggests that the REE were not significantly perturbed during alteration and metamorphism. Elements such as Zr, Y, Nb, Ti, Cr, and Ni are generally considered to be less mobile during low-temperature alteration and low-grade metamorphism (Murphy and Hynes 1986; Staudigel and Hart 1983; Grant 1986; Pearce and Norry 1979; Saunders *et al.*, 1980; Shervis 1982). For our petrogenetic interpretation we will use only those elements that are observed to be least mobile. Our samples of mafic volcanics and dykes are either least metamorphosed (dolerite) or have been metamorphosed from greenschist to amphibolites grade. Igneous trends for various major elements vs SiO_2 and Mg# in the Harker plots (Fig.3) indicate that among the major elements all the elements, except for Na_2O and K_2O, are not perturbed by post crystallization alteration.

Figure 2. CaO/Al_2O_3-MgO/10-SiO_2/100 ternary diagram

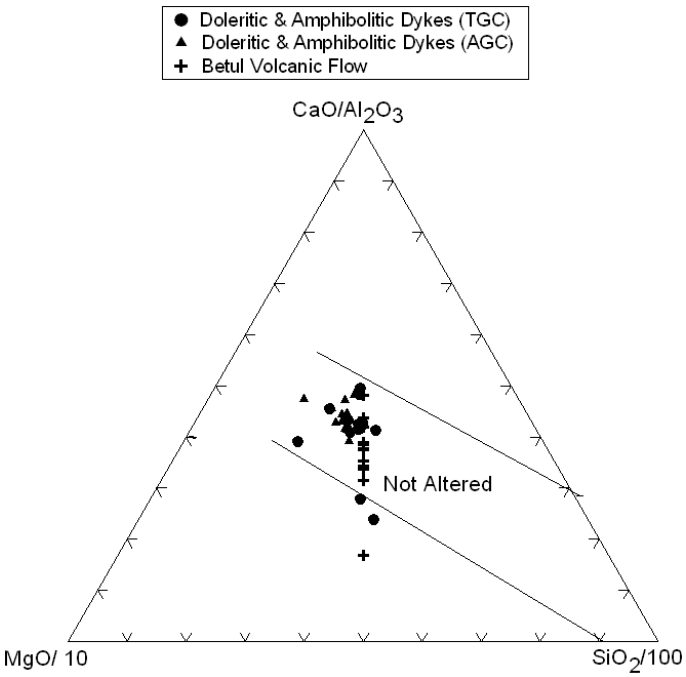

CaO/Al_2O_3-MgO/10-SiO_2/100 ternary diagram of the studied rocks sample showing their unaltered nature (Schweitzer and Kroner, 1985).

Figure 3. Harker variation diagram

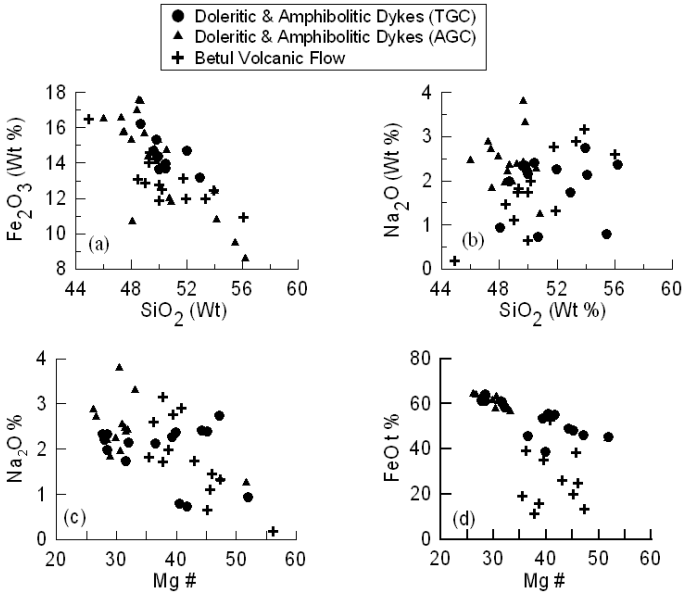

Harker variation diagram showing (a) SiO_2 vs. Fe_2O_3 wt%, (b) SiO_2 vs. Na_2O wt%, (c) Mg# vs. Na_2O wt% and (d) Mg# vs. Fe_2O_3 wt% for the mafic volcanic and dykes from TGC and AGC.

Geochemical results

Most of the samples show large variation in their elemental concentration. For example, SiO_2 which plays an important role in the determination of various rock types ranges from 44.88 wt% to 56.03 wt% with an average of 50.60 wt% for the Betul mafic volcanics. Fe_2O_3 contents in these volcanic ranges from 10.9 wt% to 16.4 wt% with an average of 12.98 wt%. Al_2O_3 varies from 8.9 wt% to 13.55 wt% with an average of 11.58 wt%. A range of variation is also observed in CaO contents. It ranges from 7.66 wt% to 14.33 wt% with an average of 11.06 wt%. TiO_3 show fewer variations from 0.43 wt% to 1.26 wt% with an average of 0.81 wt%. P_2O_5 ranges between 0.03 wt% and 0.25 wt% with an average of 0.15 wt%.

We have plotted some of the major elements against SiO_2 and Mg# to understand the differentiation processes for the studied samples. In SiO_2 and Mg # Vs Fe_2O_3 diagrams (Fig. 3a and 3d); two distinct trends are depicted by the dykes and the mafic flow samples. The dyke samples of dolerite and amphibolites of the AGC have restricted variation of FeOt and Mg# compared to those from TGC, although they overlap each other showing well defined negative trends (Fig.3d). The plots indicate tholeiitic affinity and magma evolution through olivine and pyroxene fractionation causing decrease in Mg#. The two distinct trends for the Betul mafic volcanics and the dykes probably indicate that these rocks have undergone independent petrogenetic histories. In the case of Na_2O vs Mg# and SiO_2 (Fig. 3b and 3c) no clear trend is observed which may indicate mobile nature of these elements during post crystallization processes.

Figure 4 is a series of binary plots where some of the major elements are plotted against Zr. During low grade metamorphism Zr is considered to be relatively immobile (Floyd and Lees, 1976; Winchester and Floyd. 1977; MacDonald *et al.*, 1988). Because of this reason we have used Zr content as a parameter for evaluating the elemental mobility and to understand the differentiation of magma series. CaO vs. Zr (Fig.4a) show negative relationship while TiO_2, P_2O_5, and K_2O vs Zr (Fig. 4b, 4c, and 4d) respectively show positive trend. These relationships probably indicate near primary magmatic characteristics for these major elements.

Figure 4. Binary plots of major elements vs Zr

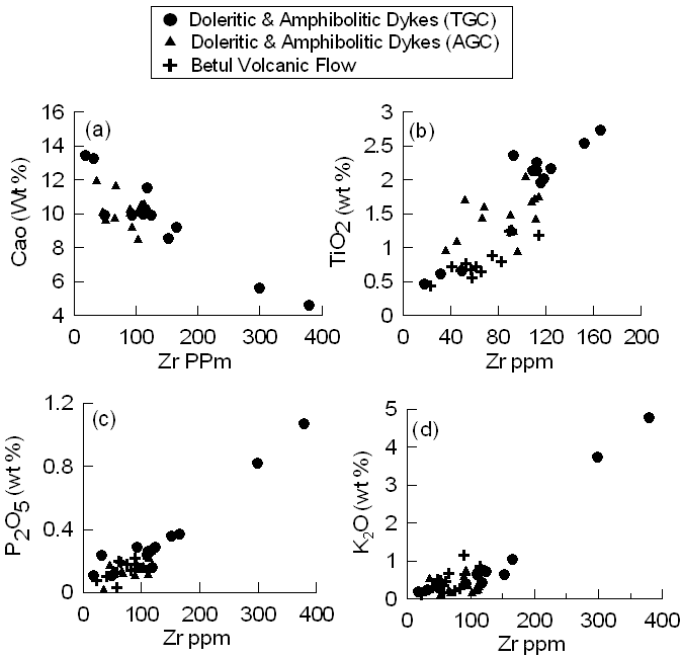

Binary plots of (a) Zr vs CaO, (b) Zr vs. TiO_2, (c) Zr vs. P_2O_5 and (d) Zr vs. K_2O for the mafic volcanic and dykes from TGC and AGC.

Figure 5 is series of binary plots where some trace such as La, Nd, Rb and Sc, are plotted against Zr, Nd is also plotted against La. All these elements have different compatibilities for basaltic /gabbroic phases (olivine, orthopyroxene, Clinopyroxene and plagioclase). These plots display magmatic trends in the form of positive relationship between Rb-Zr, La-Zr, Nd-Zr, Nd-La and with slightly perturbed negative relationship between Sc-Zr (Fig. 5b).the latter could have been affected by secondary processes to some extent. Thus most of the major and trace elements appear to have been least perturbed by post crystallisation processes and may represent near primary characteristics.

Figure 5. Binary plots of trace elements vs Zr

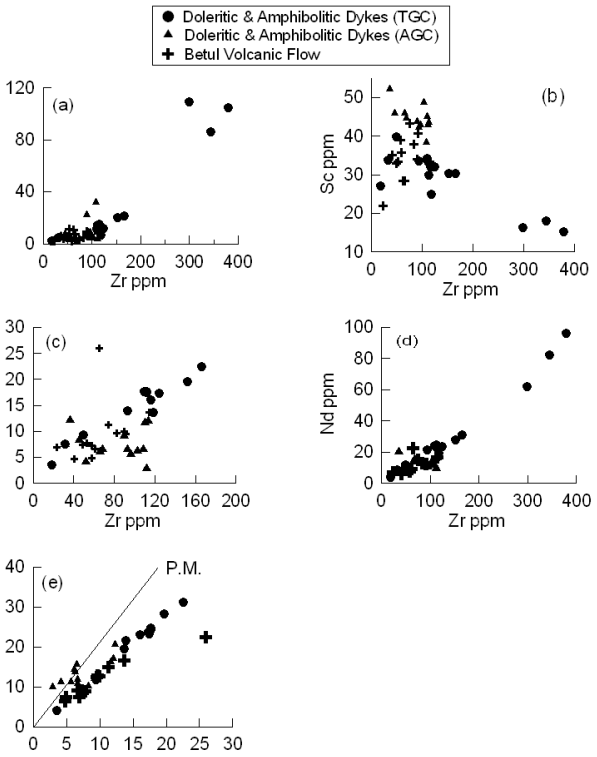

Binary plots of (a) Zr vs. Rb, (b) Zr vs. Sc, (c) Zr vs. La, (d) Zr vs. Nd and (e) La vs. Nd for the mafic volcanic and dykes from TGC and AGC.

In Figure 5d and 5e, all the data plots toward Nd and La side compared to the primitive mantle ratio line for Zr/Nd and La/Nd ratios. During melting of mantle sources Nd behaves more incompatibly than Zr and La behaves more incompatibly than Nd. Plots of the data points in these diagrams (Fig. 5d and 5e), therefore, indicate their derivation from lower degrees of partial melting of enriched mantle sources relative to primitive mantle.

Magma type

A number of simple diagram are commonly use to characterize different magma types. We reproduce two diagrams here to illustrate the nature of the Betul volcanic rocks and the dykes traversing through Tirodi and Amgaon Gneissic Complex (Fig.1). In Figure 6a, the classical AFM diagram shows a typical tholeiitic iron enrichment trend for all the studied samples. Davies *et al.* (1979) have suggested an equivalent diagram based on the immobile trace elements (Y + Zr vs 100*Ti vs Cr) which are normally immobile during alteration, does

show the samples following a clear tholeiitic trend (figure not shown here). In Fig.6b, triangular Mgo-CaO-Al_2O_3 after Viljoen *et al.* (1982), all the samples depict their tholeiitic nature.

Figure 6. AFM diagram

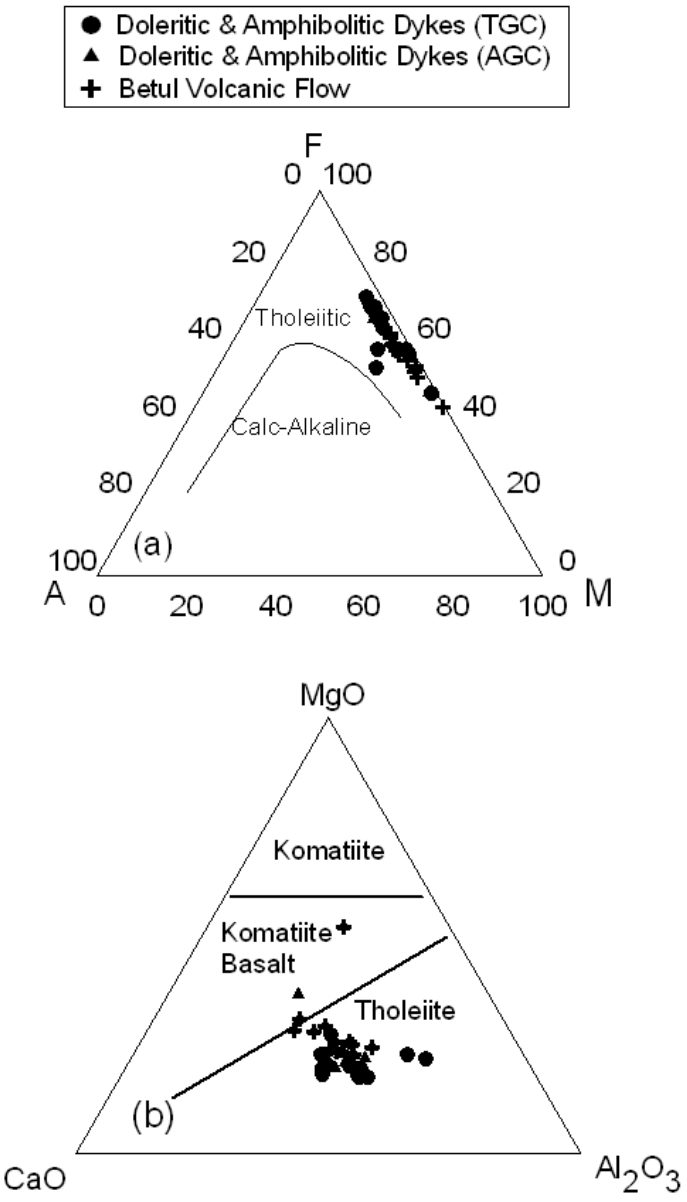

(a) Plots of A (Na_2O+K_2O) - F (FeO_t) – M (MgO) and (b) MgO-CaO-Al_2O_3 show the tholeiitic nature for the mafic volcanic and dykes from TGC and AGC. Compositional fields in (a) and (b) after Irvine and Baragar (1971) and Viljoen *et al.* (1982), respectively.

The major element classification of wt% Na_2O+K_2O versus wt% SiO_2 plot (TAS diagram after Le Bas *et al.*, 1986: Fig. 7a) is commonly used in order to classify the rock samples into basalt, basaltic-andesite, andesite, dacite and rhyolite either of sub-alkaline or alkaline series. In Figure 7a all studied samples plot within basalt and basaltic andesite fields, except for two samples (M19 and M22) which plot in basaltic trachy-andesite and trachy-andesite fields respectively. We suggest that mobile nature of Na and K may cause some deviation, but Na_2O+K_2O together may approximate to the original abundance. This inference is further substantiated by using more robust trace element criteria (Fig. 7b).

Figure 7. TAS diagram and Nb/Y vs. Zr/TiO_2 *10000 diagram

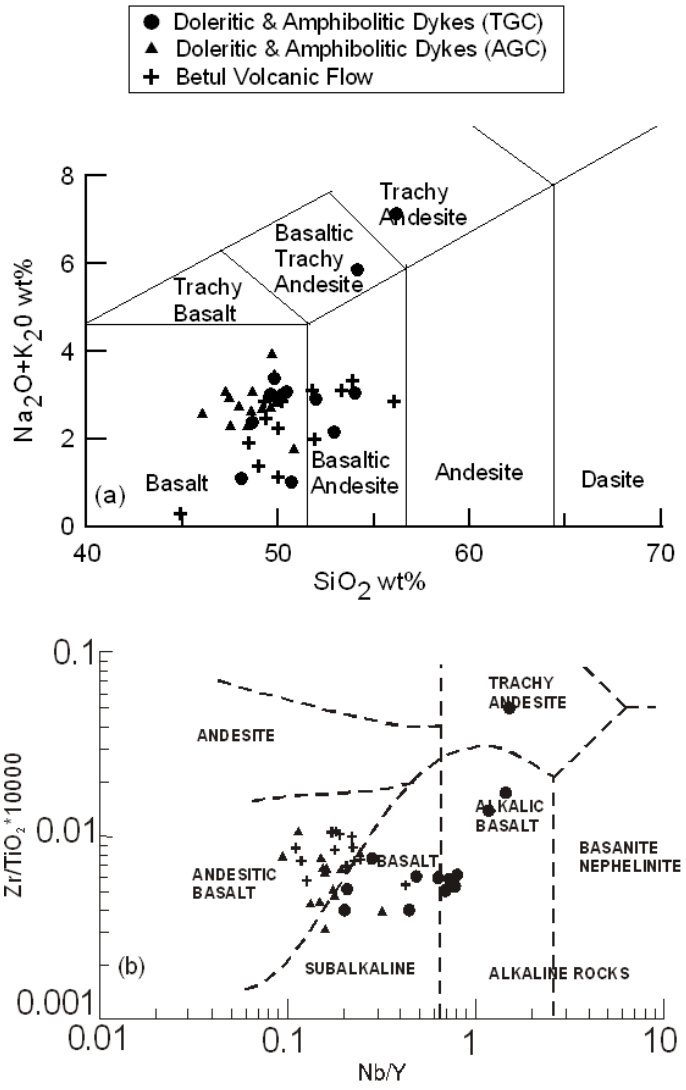

(a) Plots of SiO_2 vs. Total Alkali (TAS diagram: Le Bas *et al.*, 1986; Le Maiture, 1989) and (b) Nb/Y vs. Zr/TiO_2*10000 diagram (Wichester and Floyd, 1978) for the mafic volcanics and dykes from TGC and AGC.

Plot of Nb/Y vs. Zr/TiO_3*10000 (Fig.7b) shows the fields for common volcanic rocks (Winchester and Floyd, 1977). In this diagram our rocks plot in subalkaline series

that range from basalt to andesitic basalt except three samples that classify as alkaline rocks, like the TAS diagram (Fig. 7a). Since subalkaline series consists of tholeiitic and calc-alkaline series, the AFM plot is useful to indicate tholeiitic nature of the studied samples.

Trace element characterization

Doleritic Dyke (TGC and AGC)

Chondrite normalized rare earth elements (REE) and primitive mantle normalized spidergram plots of the studied mafic magmatic rocks are shown in Figures 8 to 10. Figures 8a and 8b represent the REE and Multi-elements patterns respectively for the doleritic dyke of the both areas. These diagrams show the enriched patterns in which sample of doleritic dyke from Tirodi Gneissic Complex (TGC) are more enriched than doleritic dykes from Amgaon Gneissic complex (AGC) which shows lower REE abundances.

Figure 8. REE and multi-element plot for doleritic dykes from TGC and AGC

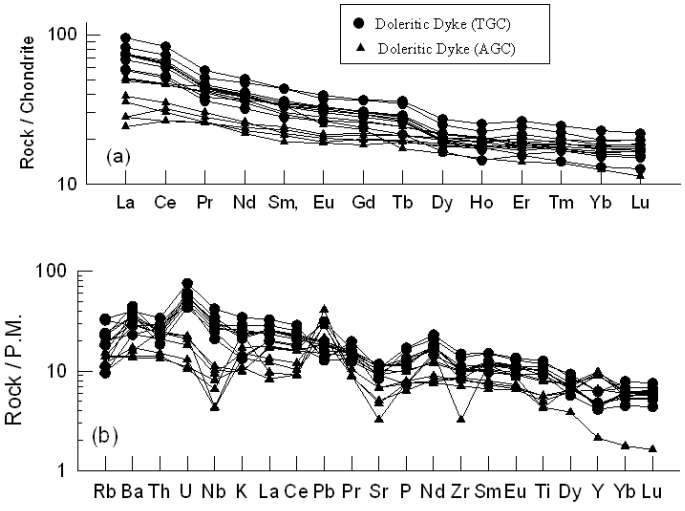

(a) C1 normalized rare earth element (REE) patterns and (b) Primitive Mantle (PM) normalized multi-element patterns for doleritic dyke from TGC and AGC. Normalizing values after Sun and McDonough (1989).

The abundance of doleritic dyke from TGC has average (ΣLREE)-(La-Sm) is 258ppm, while doleritic dyke from AGC has 161ppm, however, the average (ΣHREE)-(Gd-Lu) is 173ppm and 171ppm respectively. Average $(La/Yb)_N$ and Zr abundances are 4.25 and 138ppm respectively for doleritic dyke from TGC, while doleritic dyke from AGC has these values as 2.36 and 85ppm, indicating lesser enriched nature for the Amgaon dyke compared to those from TGC. The most primitive sample (S6) from AGC, contain higher Cr abundances of ~538ppm and Ni of ~172ppm, these abundances indicate its derivation of parental magma from a peridotite mantle source. Decrease of Ni to 22-31ppm and Cr to 35-52ppm in the in the dykes of the TGC probably indicate olivine ± spinel ± Cpx fractionation.

Normalised multi-element patterns (Fig. 8b) depict distinct patterns for dolerite from the two regions. AGC samples show strong negative anomalies for Nb and Sr and positive anomaly for Pb. There is also slight depletion of high field strength elements (HFSE) especially Ti and P. The samples from TGC show less pronounced anomalies except for strong positive U anomaly. These chemical features are commonly observed in many of the continental rift volcanic (Weaver and Tarney, 1983; Thompson *et al.*, 1983; Ahmad and Tarney, 1994).

Amphibolitic Dyke (TGC and AGC)

Figures 9a and 9b, represent the normalised REE and multi-elements patterns respectively for the amphibolitic dykes from both the areas. These diagrams show highly enriched patterns for some and not so enriched patterns for other sample of amphibolitic dyke from TGC, probably indicating their derivation from two distinct sources or they represent different degrees of partial melting of similar sources. Amphibolitic dykes from AGC region show nearly flat to slightly LREE depleted patterns, probably indicating their derivation from more primitive mantle source. The abundances of average (ΣLREE) - (La-Sm) of highly enriched sample (M19, M20 and M22) from TGC is 1125ppm and average (ΣHREE) is 221ppm. The lesser enriched samples (M23, M25 and M26) has average (ΣLREE) 94ppm and (ΣHREE) is 81ppm. The ranges of averages abundances of ΣLREE and ΣHREE for amphibolitic dyke from AGC region are 118ppm and 168ppm respectively.

Figure 9. REE and multi-element plot for amphibolite dykes from TGC and AGC

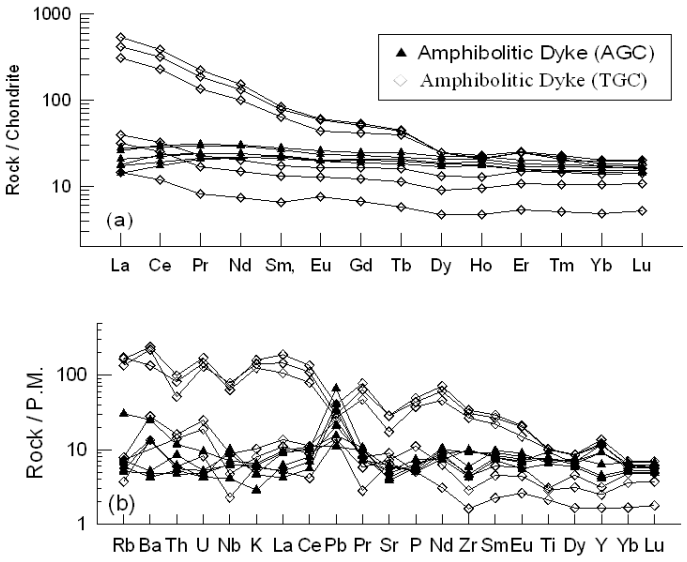

(a) C1 normalised rare earth element (REE) patterns and (b) PM normalised multi-element patterns for amphibolitic dykes from TGC and AGC. Normalizing values after Sun and McDonough (1989).

Figure 10. REE and multi-element plot for Betul mafic volcanics

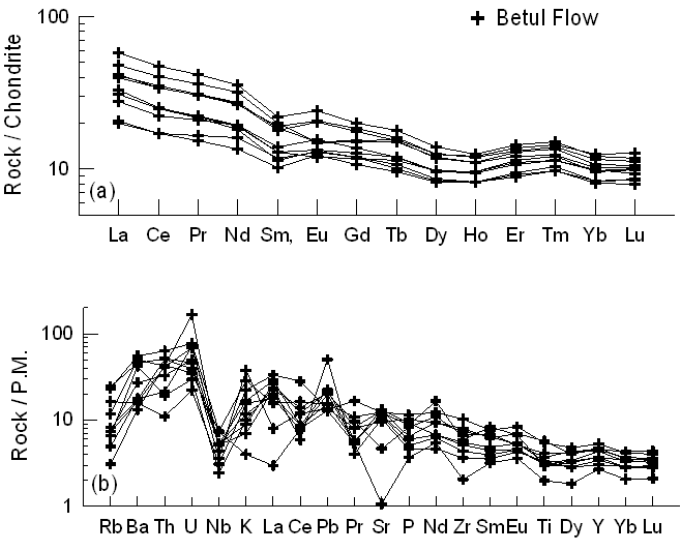

(a) C1 normalized rare earth element (REE) patterns and (b) Primitive Mantle normalized multi-element patterns for Betul volcanic flows. Normalizing values after Sun and McDonough (1989).

Betul Volcanic Flow

Chondrite-normalized rare earth elements (REE) and primitive mantle normalized incompatible multi-element patterns for the Betul mafic volcanic are shown in Figures 10a and 10b. These diagrams show enriched pattern for incompatible trace elements especially for the light rare earth elements (LREE) and large ion lithophile elements (LILE). The LREEs are about 20-60 times chondrite and the HREEs are about 10 times chondrite for the mafic volcanic rocks of the area. The multi-element patterns depict negative Nb, P and Ti anomalies for the Betul volcanic rocks (Fig. 10b). In general the REE patterns show less fractionated to nearly flat MREE-HREE patterns. The negative Nb, P and Ti anomalies commonly observed in many Phanerozoic continental rift volcanics (Weaver and Tarney, 1983., Thompson et. al., 1983., Ahmad and Tarney, 1994., Ahmad and Rajamani, 1991., and Ahmad and Bhat, 1987), observed anomalies in our sample probably indicate a similar tectonic setting our study area.

The Nb/La and Nb/Ce ratios for the Betul volcanic range from 0.120 to 0.743 and 0.366 to 0.62 respectively. La/Yb and La/Sm ratios range from 3.35 to 18.68 and 2.71 to 7.02. The average values of Nb/La, Nb/Ce, La/Yb and La/Sm for the Betul volcanic samples are 0.422, 0.20, 6.06, and 3.90 respectively. The REE patterns are characterized by fractionated trends (La_N/Yb_N = 1.44 to 11.83) probably indicating varying degree of partial melting. No Eu anomaly is observed in any of the REE patterns indicating little role of plagioclase in their genesis.

Sm/Yb is susceptible to the presence or absence of residual garnet in the source. The Sm/Yb ratio varies from 1.10 to 2.65 with an average of 1.47 and the La/Sm ratios are variable between about 2.71 to 7.02 for the Betul mafic samples, which may indicates generation of magma in the absence of garnet, probably indicating shallow depths of magma generation (Huang *et al.*, 2000).The absence of residual garnet in the source is also supported by the REEs patterns (Fig. 10a) which shows the less depletion of HREE. The Nb/La values ranges from 0.12 to 0.74 whereas La/Sm ratio varies between 2.71 to 7.02. Some of the samples show extremely low Nb/La ratios probably suggesting fractionation of titanites or their stabilization in the residual source.

Average (Nb/La) and (Nb/Ce) ratios of the doleritic dyke of TGC ranges 1.22 and 0.56 while the ranges for AGC dyke are 0.61 and 0.25 respectively. These values for doleritic dykes for the AGC are much lower compared to Nb/La and Nb/Ce values of primitive mantle which are 1.03 and similar to 0.40, respectively. Nb/La and Nb/Ce ratios for TGC dolerite is close to primitive mantle ratios. The negative Ba anomaly in some samples may be due to either alteration or fractionation of feldspar, hornblende and biotite during genesis of these rocks because Ba substitutes for K in K-feldspar, hornblende and biotite.

Figure 11 shows the multi-element and REE plots of averages of all the studies samples from different groups. The amphibolites samples of the TGC have much higher LREE/HREE ratios and LREE enrichment compared to all the samples studied. The dolerite samples from the TGC is less enriched with lower LREE/HREE ratios than the amphibolites from the same area but have higher abundance and LREE/HREE ratios than samples from the AGC and the Betul mafic volcanic. The amphibolite and dolerite samples from ACG have close similarity in terms of LREE abundance and LREE/HREE ratios, probably indicating that they share common source characteristics and petrogenetic histories. Samples of the Betul mafic volcanic have lower LREE abundances and LREE/HREE ratios than all the other studied samples, however, their patterns are parallel to the dolerite and amphibolites samples of the TGC, probably indicating derivation of the volcanic by higher degrees of partial melting of similar sources as for amphibolites and dolerite from the TGC.

Figure 11. Multi-element and REE and for averages of all group of samples

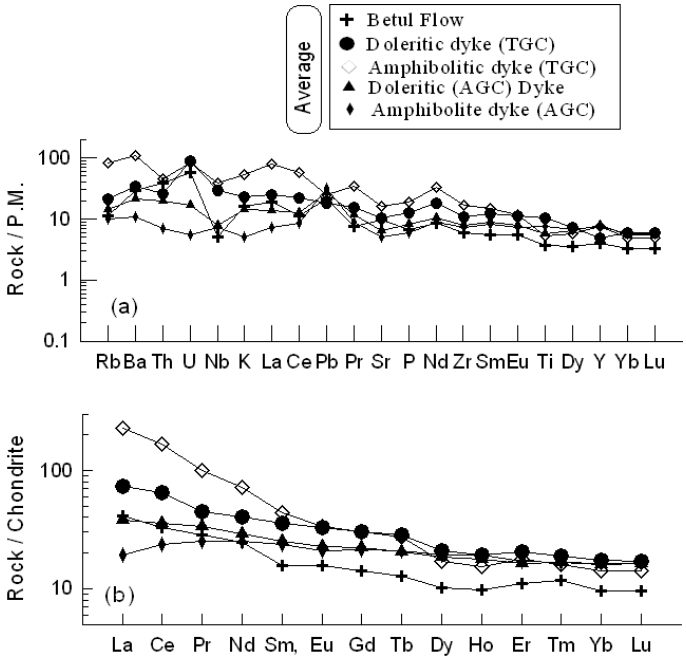

(a) Primitive mantle normalized multi-element patterns, and (b) C1 normalized rare earth element (REE) patterns of the average values for the various groups of mafic magmatic rock samples under consideration. Normalizing values after Sun and McDonough (1989).

The studied samples are plotted in the Zr/Y vs Zr diagram (Fig.12) of Floyd (1993) that shows two calculated partial melting curves (after Drury, 1983) corresponding to two distinct source mineralogy (Curve I: olivine 60% + orthopyroxene 20% + clinopyroxene 10% + plagioclase 10%; Curve II: olivine 60% + orthopyroxene 20% + clinopyroxene 10% + garnet 10%) for Archean mantle source (Sun and Nesbitt, 1977). Most of the doleritic and amphibolitic dyke of TGC and Betul volcanic flow samples plot along curve II indicating derivation from common sources by varying degrees of partial melting. The lateral variation of the TGC dykes probably indicates subsequent fractionation of Cpx ±O1+Plag during the evolution of the magma. The volcanic samples appear to represent relatively higher degrees of partial melting of similar source but appear to have suffered little fractionation of these phases. The AGC samples plot closer to or below the curve I, probably indicating derivation by higher degrees of partial melting at shallower source region.

Figure 12. Zr/Y vs. Zr diagram

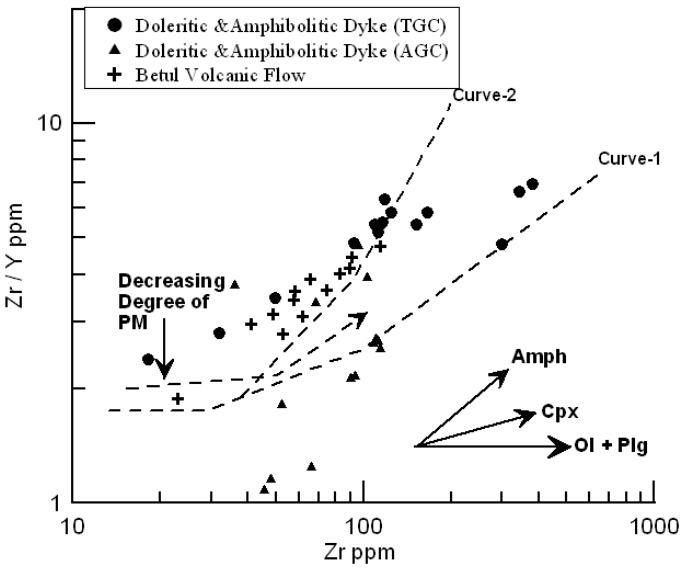

Binary plot of Zr/Y vs. Zr for the mafic volcanic and dyke samples of study area. Melting Curve (I and II) are after Drury (1983); vectors for fractional crystallization are after Floyd (1993).

In Figure 13a samples are plotted in Ni-Ce space showing calculated partial melting curves for primitive mantle (PM) and modified mantle (MM) and a line for fractional crystallisation after Rajamani *et al.* (1989). It is observed that none of the samples plot along the partial melting curve for PM, but some of the AGC samples do plot closer to that for the MM. All the samples of the TGC plot parallel to the partial melting curve for the MM but with much lower Ni abundances of ~30ppm. This probably indicate their derivation from MM type source followed by severe fractional crystallisation of olivine ± pyroxens ± plagioclases or they are derived from low degrees of partial melting of mantle sources much more enriched than MM shown in Figure 13a.

Figure 13. Ni-Ce and Ce-Nd diagrams

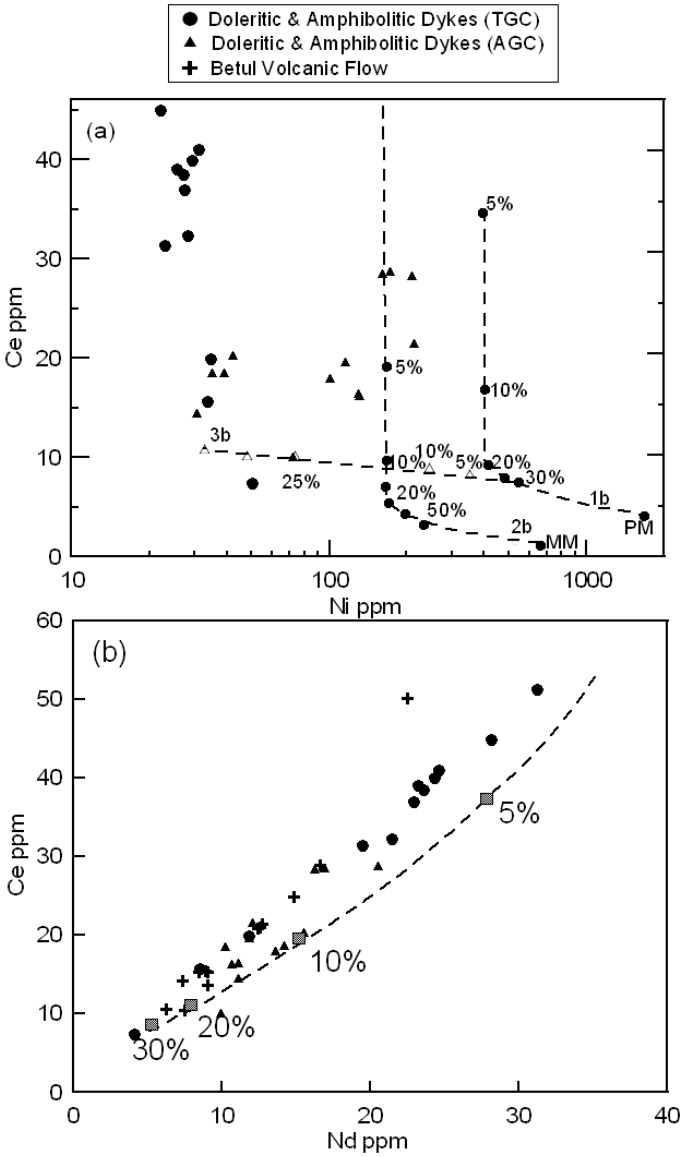

(a) Ni vs Ce plots for the studied samples, lines 1b and 2b are calculated batch melting path for Primitive Mantle (PM) and Modified Mantle (MM), respectively. Line 3b is calculated melt evolution curves for the fractional crystallization (after Rajamani *et al.*, 1989) and (b) Nd vs Ce plot for the mafic magmatic samples of the study area. Calculate partial melting curve (after Ahmad and Tarney, 1991).

In Figure 13b samples are plotted in Ce-Nd diagram, where calculated partial melting curve for primitive mantle is shown after Ahmad and Tarney (1991). All the samples plot parallel to the partial melting curve but on the Ce side with higher Ce/Nd ratio than primitive mantle, probably indicating their derivation from enriched mantle sources as indicated by many other diagrams discussed above. The amphibolites and dolerite samples

from TGC show higher abundances of Ce and Nd indicating their derivation from lower (~5-10%) degrees partial melting of an enriched mantle source. The amphibolites and dolerite from the AGC do follow the same partial melting curve but have lower abundance of Ce and Nd than those from TGC, probably indicating derivation of the AGC samples by relatively higher degrees of partial melting. The Betul mafic volcanic samples plot on the same curve but with much lower abundances for Ce and Nd, probably indicating derivation by relatively higher degrees of partial melting than amphibolites and dolerite from the same area (TGC).

Above discussion based on the trace elements characteristics clearly indicate that the studied samples are derived from enriched mantle sources by varying degrees of partial melting followed by fractionation of olivine, pyrocxene and plagioclases for some of the doleritic and amphibolitic samples. The Betul mafic volcanic appear to have suffered little fractional cryatallisation compared to their hypabyssal equivalents.

The tectonic discriminant Ti-V diagram (Fig. 14) after Shervais (1982) is also being used to understand the tectonic setting of the studied samples. The basis of this plot is the variation in the crystal/liquid partition coefficients for vanadium, which range with increasing oxygen fugacity from >1 to <<1. Since the partition coefficient for Ti is almost always <<1, the depletion of V relative to Ti is a function of the fO_2 of the magma and its source, the degree of partial melting and subsequent fractional crystallization. Most of the studied samples plot in the "Within Plate Basalt (WPB)"/ Rift volcanic field, indicating their emplacement in a rift tectonic environment. This is well supported by the associated continentally derived sediments and huge granitoid basement.

Figure 14. Ti/1000 vs. V diagram

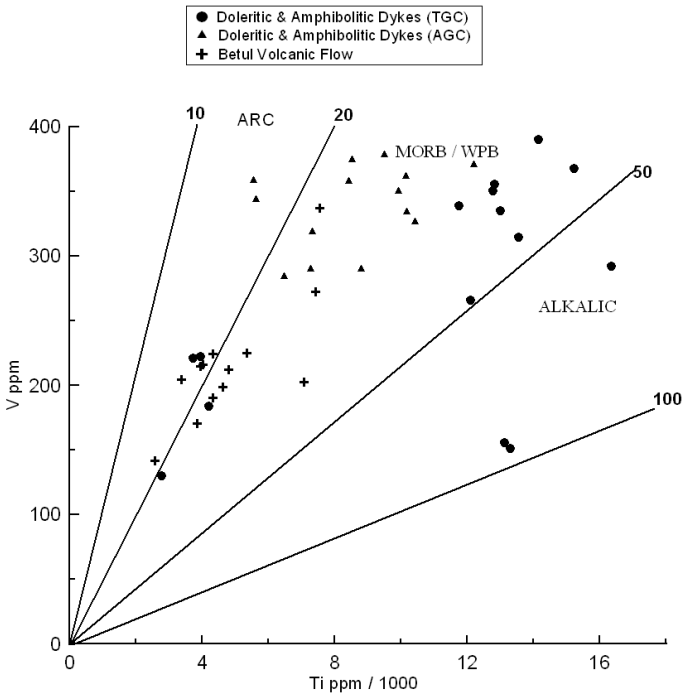

Binary plots of Ti/1000 vs. V diagram indicating within plate setting for the studied mafic magmatic rock samples of the TGC and AGC area. (after Shervais, 1982).

Acknowledgment

We thank DST, New Delhi for the grant of funds under ILTP and SERC projects to TA. We also thank the University of Delhi for all the facilities and partial funding under the Minor Project given to TA. We thank colleagues of NGRI geochemistry laboratory for the analytical support. We thank Ms. Sangeeta Gupta for the assistance in finalising the manuscript. Mukesh Kumar Mishra is especially thanked for the help during the field work.

References

Acharyya, S.K., Roy, A., 2000. Tectonothermal history of the Central Indian Tectonic Zone and reactivation of major faults/shear zones. J. Geol. Soc. India 55, 239-256.

Ahmad, T., Longjam, K.C., Fouzdar, B., Bickle, M.J., Chapman, H.J., 2009. Petrogenesis and tectonic setting of bimodal volcanism in the Sakoli Mobile Belt, Central Indian shield. Island Arc 18, 155-174.

Ahmad, T., Bhat, M.I., 1987. Geochemistry and Petrogenesis of Mandio Darla volcanics, northwestern Himalayas, Precambrian Research 37, 231-256.

Ahmad, T., Rajamani, V., 1991. Geochemistry and petrogenesis of the basal Aravalli volcanics near Nathdwara, Rajasthan, India. Precambrian Research 49, 185-204.

Ahmad, T., Tarney, J. 1991. Geochemistry and Petrogenesis of Garhwal volcanic: implications for evolution of the north Indian lithosphere. Precambrian Research 50, 69-88.

Ahmad, T., Tarney, J., 1994. Geochemistry and petrogenesis of late Archaean Aravalli volcanics, basement enclaves and granitoids, Rajasthan. Precambrian Res. 65, 1-23.

Balaram, V., Ramesh, S. L., Anjaiah, K. V., 1996. New trace and REE data in the thirteen GSF reference samples by ICP-MS. Geostandards Newsletter. 20, 71-78.

Bickle, M.J., 1990. Mantle evolution. In: Hall, R.P. and Hughes, D.J. (Eds.) Early Precambrian Basic Magmatism. Blackie, Glasgow (and Chapman and Hall, New York), 111-135.

Campbell, I.H., Griffiths, R.W., 1990. Implication of mantle plume structure for the evolution of flood basalt. Earth and Planetary Science letters 99, 79-93.

Chattopadhyay, A., Bandyopadhyay, B. K., Khan, A. S., 2001. Geology and structure of the Sausar fold belt: A retrospection and some new thoughts. Geological Survey of India, Special Publication. 64, 251-264.

Cloud, P., 1976. Major features of crustal evolution. Geological Society of S.Africa., Alex L. du Toil Memorial Lecture Series 14, 33.

Condie, K.C., 1985. Secular variation in the composition of basalts: an index to mantle evolution. Journal of Petrology 28, 545-563.

Condie, K.C., 1986. Geochemistry and tectonic settings of early Proterozoic supracrustal rocks in the south western United States. Journal of Geology 94, 845-864.

Condie, K.C., 1989. Geochemical changes in basalts and andesites across the Achaean-Proterozoic boundary: Identification and significance. Lithos 23, 1-18.

Drury, S.A., 1983. The Petrogenesis and tectonic setting of Archean metavolcanics from Karnataka state, south India. Geochim. Cosmochim. Acta 47, 317-329.

Floyd, P.A., 1993. Geochemical discrimination and Petrogenesis of alkali basalt sequences in part of the Ankara melange, central Turkey. Journal of the Geological Society 150, 541-50.

Floyd, P. A., Lees, G. J., 1976. Basic intrusion in the Ordovician of North Wales-geochemical data and tectonic settings. Proceedings of the Geological Association. 87:4, 389-400.

Floyd, P.A., Winchester, J.A., 1978. Identification and discrimination of altered and metamorphosed volcanic rocks using immobile elements. Chemical Geology 21(3-4), 291-306.

Grant, J.A., 1986. The isocon diagram- a simple solution to Gresens, equation for metasomatic alteration. Economic Geology 81, 1976-1982.

Hargraves, R.B., 1981. Precambrian tectonic style: A libral uniformitarian interpretation. In: Kroner A. (Ed.) Precambrian Plate Tectonics, 21-25.

Huang,Yiming., Hawkesworth, Chris., Smith, Ian., Calsteren, Peter van., Black, Philippa., 2000. Geochemistry of late Cenozoic basaltic volcanism in Northland and Coromandel, New Zealand: implications for mantle enrichment processes. Chemical Geology 164, 219-238.

Irvine, T.N., Baragar, W.R.A., 1971. A guide to the chemical classification of the common volcanic rocks. Can. Jour. Earth Sci. 8, 523-548.

Jain, S.C., Yedekar, D.B., Nair, K.K.K., 1991. Central Indian Shear Zone: a major Precambrian crustal boundary. Journal of Geological Society of India 37, 521–548.

Kroner, A., 1981. Precambrian plate tectonics. In: A. Kroner, Editor. Precambrian Plate tectonics; Developments in Precambrian Geology 4. Elsevier, Amsterdem. 57-90.

Le Bas, M.J., Le Maitre, R.W, Streckeisen, A., Zanettin B., 1986. A chemical classification of volcanic rocks based on the total alkali-silica diagram. Journal of Petrology 27, 745-50.

Ludden, J.N., Thompson, G., 1979. An evaluation of the behaviour of the rare earth elements during the weathering of sea-floor basalt. Earth and Planetary Science letters 43, 85-92.

Macdonald, R., Millward, D., Beddoe-Stephens, B., Laybourn-Parry, J., 1988. The role of tholeiitic magmatism in English Lake District: evidence form dyke in Eskdace. Mineral Mag. 52, 459-472.

Mason, B., Moore, C.B., 1982. Principles of Geochemistry (4th Edition). John Wiley & Sons.

McCulloch, M.T., Wasserburg, G.J., 1978. Sm-Nd and Rb-Sr chronology of continental crust formation. Science 200, 1003-1011.

Moorbath, S., 1977. Ages, isotopes and evolution of Precambrian continental crust. Chemical Geology 20, 151-187.

Murphy, J.B., Hynes, A.J., 1986. Contrasting secondary mobility of Ti, P, Zr, Nb and Y in two meta-basaltic suites in the Appalachians. Canadian Journal of Earth Sciences 23, 1138-1144.

Naqvi, S.M., 1981. The oldest supracrustal of the Dharwar Craton, India. Journal of the Geological Society of India 22, 458-469.

Pearce, J.A., Norry, M.J., 1979. Petrogenetic implications of Ti, Zr, Y, and Nb variations in volcanic rocks. Contributions to Mineralogy and Petrology 69, 33-47.

Pharaoh, T.C., Beckinsale, R.D., Rickard, D., (Eds.) 1987. Geochemistry and Mineralization of Proterozoic Volcanic Suites. Geological Society, London Special Publication 33, 552.

Rajamani, V., Shirey, S.B., Hanson, G. N., 1989. Fe-rich Archaean tholeiites derived from melt enriched mantle sources: Evidence from the Kolar Schist Belt, South India. Jour. Geol. 97, 487-501.

Sarkar S.N., Trivedi J.R., Gopalan K., 1986. Rb-Sr whole rock and mineral isochron age of the Tirodi gneiss, Sausar Group, Bhandara district, Maharashtra. Journal of Geological Society of India 27, 30-37.

Saunders, A.D., Tarney, J., Weavers, S.D., 1980. Transverse geochemical variation across the Antarctic Peninsula: Implication for the genesis of calc-alkaline magmas. Earth and Planetary Science Letters 46, 344-360.

Schweitzer, J., Kroner, A., 1985. Geochemistry and petrogenesis of early Proterozoic intracratonic volcanic rocks of the Ventersdrop Supergroup, South Africa. Chemical Geology 51, 265-288.

Shervais, J.W., 1982. Ti-V plot and the petrogenesis of modern and ophilitic lavas. Earth and Planetary Science Letters 59(1), 101-118.

Staudigel, H., Hart, S.R., 1983. Alteration of basaltic glass: mechanism and significance for the oceanic crust-sea water budget. Geochimica Cosmochimica Acta 47, 37-50.

Stein, J. H., Hannah, J. L., Zimmerman, A., Markey, R. J., Sarkar, S. C., Pal, A. B., 2004. A 2.5 Ga porphyry Cu–Mo–Au deposit at Malanjkhand, Central India: implications for Late Archean continental assembly. Precambrian Research 34, 89-226.

Sun, S.S., McDonough, W.F., 1989. In: Saunders, A.D., Norry, M.J. (Eds.), Chemical and isotopic systematics of oceanic basalts: implications for mantle composition and processes Magmatism in Ocean Basins. Geological Society Special Publication 42, 313-345.

Tarney, J., Windley, B.F., 1977. Chemistry, thermal gradients and evolution of the lower continental crust. Journal of Geological Society, London 124, 153-172.

Taylor, S.R., 1987. Geochemical and petrological significance of the Achaean-Proterozoic boundary. In: Pharaoh, T.C., Beckinsale, R.D.and Rickard, D., (Eds.) Geochemistry and Mineralization of Proterozoic Volcanic Suites, Geological Society, London, Special Publication 33, 3-8.

Taylor, S.R., McLennan, S.M., 1985. The Continental Crust: Its Composition and Evolution. Blackwell Scientific Publications, Oxford.

Thompson, R.N., Morrison, M.A., Dickin, A.P., Hendry, G.L., 1983. Continental flood basalts: arachmids rule OK? Continental Basalts and Mental Xenoliths (Hawkesworth, C.J. and Norry, M.J., eds.), Shiva Publ., Nantwich 155-185.

Viljoen, M.J., Viljoen, R.P., Pearton, T.N., 1982. The nature and distribution of Archean komatiite volcanics in South Africa (in komatiites) George Allen and Unwin, London, United Kingdom 53-79.

Weaver, B.L., Tarney, J., 1983. Trace element geochemistry of basalts recovered by DSDP Leg 82; implications for mantle heterogeneity. In American Geophysical Union; Spring meeting. Eos, Transactions, American Geophysical Union 64(18), 345.

White R.S., McKenzie, D.P., 1989. Magmatism at rift zones. The generation of volcanigenic continental margins and flood basalts. Journal of Geophysical Research 94, 7685-7729.

Windley, B.F., 1982. The evolving continents. John Wiley. 399.

Winchester, J.A., Floyd, P.A., 1977. Geochemical discrimination of different magma series and their differentiation products using immobile elements. Chemical Geology 20, 325-344.

Yedekar, D.B., Jain, S.C., Nair, K.K.K., Dutta, K.K., 1990. The Central Indian collision suture. Precambrian of Central India, Geol. Survey of India Special Publication 28, 1-37.

Yedekar, D.B., Karmalkar, N., Pawar, N.J., Jain, S.C., 2003. Tectonomagmatic evolution of Central Indian terrain. Gondwana Geol. Magz. Spl. 7, 67-88.